Journal of Volcanology and Geothermal Research 206 (2011) 121–135

Contents lists available at ScienceDirect

Journal of Volcanology and Geothermal Research

journal homepage: www.elsevier.com/locate/jvolgeores

Identifying potentially active volcanoes in the Andes: Radiometric evidence for late Pleistocene-early Holocene eruptions at Volcán Imbabura, Ecuador

J.L. Le Pennec [a,b,c,*], A.G. Ruiz [d], J.P. Eissen [a,b,c,1], M.L. Hall [d], M. Fornari [e]

[a] Clermont Université, Université Blaise Pascal, Laboratoire Magmas et Volcans, BP 10448, F-63000 Clermont-Ferrand, France
[b] CNRS, UMR 6524, Laboratoire Magmas et Volcans, 5 rue Kessler, 63038 Clermont-Ferrand cedex, France
[c] IRD, R 163, Laboratoire Magmas et Volcans, 5 rue Kessler, 63038 Clermont-Ferrand cedex, France
[d] Instituto Geofísico, Escuela Politécnica Nacional (IG-EPN), Ap. 17-01-2759, Quito, Ecuador
[e] IRD, UMR GéoAzur, Université Nice-Sophia Antipolis, Parc Valrose, 06108 Nice, France

ARTICLE INFO

Article history:
Received 24 February 2011
Accepted 7 June 2011
Available online 28 June 2011

Keywords:
Active volcanoes
Radiometric dating
Imbabura volcano
Ecuador

ABSTRACT

Recent eruptions from volcanoes with no previously known historical activity in Chile and Indonesia have raised the importance of the early identification of potentially active centers for the purpose of hazard assessment. Here we bring radiometric evidence (^{14}C,^{39}Ar–^{40}Ar) of previously unrecognized but significant magmatic activity at partly eroded Imbabura volcano (Ecuador) in late Pleistocene to early Holocene times, on whose perimeter live more than 300,000 persons. Following an effusive stage from 50 to 30 ka with the emplacement of andesitic lava flows on different flanks of its edifice, the activity became explosive with the generation of andesitic block-and-ash flows on its eastern side, beginning at ~35 ka cal BP. Subsequently a flank collapse associated with a volcanic blast occurred on the volcano's SW flank at ~30 ka cal BP. The resulting debris avalanche and blast breccias cover an area now heavily populated around San Pablo Lake and its source was later concealed by successive dome building episodes at Huarmi which produced ~2.8 km^3 of silicic andesite. Renewed dome activity at the edifice's Taita summit occurred at ~17 ka cal BP and continued intermittently into early Holocene times, as indicated by pyroclastic flow deposits overlying a palaeosoil dated at ~9 ka cal BP. In summary, this study reveals an eruptive behavior characterized by a low recurrence rate but with quite large eruptions, a pattern which is also observed at other silicic volcanoes of Ecuador's Western Cordillera. It is now imperative to reconsider the origin and source of the many tephra layers catalogued in Holocene lacustrine sediments in the Imbabura area. Tephra and lava volume estimates for Imbabura volcano converted to Dense Rock Equivalent values yield a minimum magmatic output rate of 0.13 km^3/ka in the past 35,000 years, which argues for sustained magma production for this volcano in recent geological times. The Imbabura example thus raises the question of how to improve population preparedness for volcanoes with infrequent eruptions, and how to guide authorities' decisions concerning the development of urban areas and infrastructures near presently inactive but potentially highly dangerous volcanoes.

1. Introduction

The modest-sized Chaitén volcano, southern Chile, had no recorded historical eruptions and remained very poorly known before its reactivation in 2008 (Simkin and Siebert, 1994). The sudden explosive eruption in May 2008 was surprisingly violent (VEI 4 according to Watt et al., 2009) and downwind ash-falls impacted public health and air traffic, while lahars severely damaged the city of Chaitén, south of the volcano. In August–September 2010, Sinabung volcano in northern Sumatra, Indonesia, also erupted for the first time in historical time, forcing the evacuation of 30,000 people. Similarly, older powerful and devastating eruptions of Pinatubo in 1991 (Philippines; Newhall et al., 1996), Tambora in 1815 (Indonesia; Stothers, 1984) and Huaynaputina in 1600 (Peru; Thouret et al., 1997) have occurred at volcanoes with no previously known historical activity. These examples highlight the importance of distinguishing potentially active from definitively extinct volcanoes for the purpose of hazard assessment. Because the current consensus defines a potentially active volcano as a system that had eruptive activity in the Holocene, i.e. in the past 10 ka (Simkin and Siebert, 1994; Szakács, 1994; Siebert et al., 2011), it is necessary to complete the volcanological information beyond the historical archives by investigating the geological record of the past millennia. However, in practice this can prove difficult for lack of datable material, poor accessibility, etc., and the distinction may be complicated for volcanoes with very low eruptive recurrence rates, in which eruption episodes are separated by thousands of years. Nonetheless, it is

* Corresponding author at: IRD, R 163, Laboratoire Magmas et Volcans, 5 rue Kessler, 63038 Clermont-Ferrand cedex, France.
E-mail address: jeanluc.lepennec@ird.fr (J.L. Le Pennec).
[1] Deceased.

0377-0273/$ – see front matter © 2011 Elsevier B.V. All rights reserved.
doi:10.1016/j.jvolgeores.2011.06.002

expected in terms of risk assessment that populations probably react in a similar way to reactivating volcanoes with no known historical eruptions, or no known Holocene events.

The continental volcanic arc of Ecuador comprises about 55 young strato-volcanoes, of which twenty have been active in the Holocene and eleven since the Spanish Conquest in AD 1533. Most centers sit in or near the populated Inter-Andean corridor, a depressed N-S-trending area located between the western and the eastern cordilleras of Ecuador (Hall et al., 2008). Several regular strato-cones with "fresh-looking" morphology show small incising gullies which indicate sustained activity in past centuries to thousands of years. This is the case of Cotopaxi (Hall and Mothes, 2008b) and Tungurahua volcanoes (Hall et al., 1999; Le Pennec et al., 2008). Other poorly studied volcanoes show deep erosion features, including glacial valleys, suggesting that they are mainly of Pleistocene age and possibly definitively extinct (e.g. Pasochoa, Sincholagua, Ruminahui, Hall et al., 2008). Some volcanoes display geomorphological features of both potentially active and extinct edifices, and this includes volcanic complexes as Pichincha (Robin et al., 2010), and Mojanda Fuya-Fuya (Robin et al., 2009). This is also the case of the Imbabura volcanic complex, which has no recorded Holocene eruptions. Although Imbabura was locally considered as a potentially active volcano (von Hillebrandt et al., 1991), it was not included in the early Catalogue compiled by Simkin and Siebert (1994), probably because of the lack of dated material. In this note we present the first evidence supporting magmatic eruptions at Imbabura volcano from late Pleistocene to early Holocene times. We document the age and style of the activity and show that noticeable debris flows have recurrently swept the flanks of the edifice in late Holocene times. These findings have important implications for natural hazard evaluation as the volcano sits in a densely populated area, near the provincial capital of Ibarra.

2. Geological background and previous studies

Quaternary volcanism in the Northern Volcanic Zone of the Andes has developed in Colombia and Ecuador as the result of the subduction of the Nazca oceanic plate below the South American continental margin (Fig. 1). In Ecuador more than 50 andesitic to rhyolitic volcanic centers have formed in Quaternary times along the N-S-trending cordilleras and in the Inter-Andean Corridor, thus posing a major threat upon the rapidly growing population (Hall et al., 2008). The Imbabura Volcanic Complex (IVC) is located in the eponym province about 60 km N of Quito, Ecuador's capital city. It is surrounded by several large stratovolcanoes including Cayambe to the SE, Cusín to the S, Mojanda Fuya-Fuya to the SW, Cuicocha to the W and Cotacachi and Huanguillaro-Chachimbiro to the NW (Fig. 2). The IVC sits immediately S of the provincial city of Ibarra (250,000 inhabitants) and near other large towns, including San Antonio de Ibarra, Atuntaqui, Otavalo, and San Pablo del Lago, which are found all along the northwestern to southwestern piedmonts of the complex (Fig. 2). The N-S diameter of the volcanic complex measures ~16 km with an E-W diameter of ~14 km. Its central edifice is called Taita Imbabura ("Father Imbabura" in Quechua language, 4620 m above sea level, asl) with basal diameters of 10×11 km (Fig. 3a). The smaller Cubilche edifice (3826 m asl) located SE of the main Taita center displays a horseshoe-shaped amphitheater opened to the N (Fig. 2), which is a result of a flank failure event of unknown age. To the NE of Taita volcano is a steep-sided satellite peak called El Artezon (4137 m asl, Fig. 2). A prominent "fresh-looking" lava dome complex occurs on the southwestern side of the main Taita edifice, and is called Huarmi Imbabura (the "Son of Imbabura," 3926 m asl, Fig. 3a). The IVC is largely vegetated and covered by thick andisoils locally known as "Cangahua," an ash-rich eolian deposit of late Pleistocene age widespread in the Ecuadorian highlands (Hall and Mothes, 1996) and that greatly hinders geological investigations by covering most outcrops. The drainage of the volcanic complex has a broad radial pattern, beginning on Taita's summit and descending eastward to the Tahuando River (e.g. via the conspicuous Rumipamba fan), and south westward to San Pablo Lake, and northwestward to the Ambi River (Fig. 2).

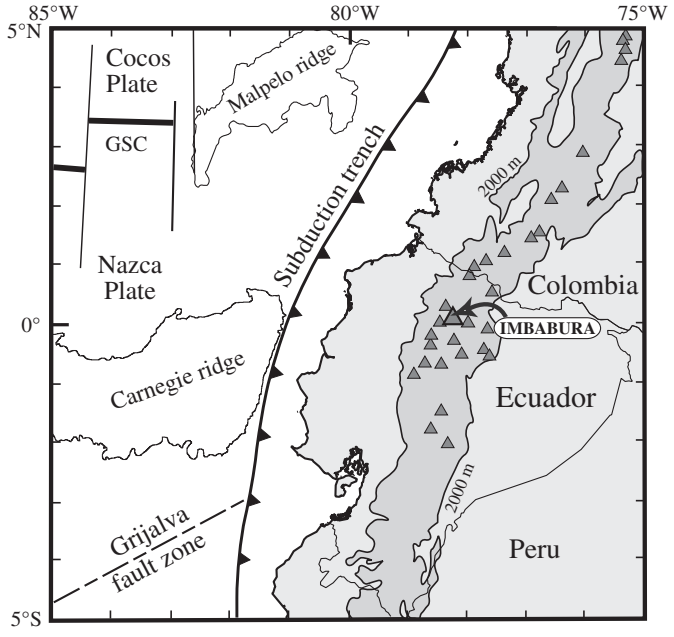

Fig. 1. Geodynamic setting and distribution of the Quaternary volcanic centers in the Northern Volcanic Zone of the Andes. The Andean Cordilleras are delineated by the 2000 m asl contour and dark gray shading. GSC is the Galapagos Spreading Center.

Previous studies of the Imbabura complex (von Hillebrandt, 1989; Hall and Beate, 1991; Ruiz, 2003; Ruiz et al., 2003) indicate that the eastern part of the IVC sits near volcanic rocks of Mio-Pliocene age known as the Angochagua (6.3 Ma) and Pugarán (5.0 Ma) series (Boland et al., 2000). In addition, the occurrence of light-colored angular xenoliths in lavas of the Cubilche and nearby Cunrru centers shows that the eastern part of the complex is underlain by sienitic to dioritic rocks, while under the western side of the complex IVC lavas carry xenoliths of schists and gneisses belonging to the Mesozoic terranes of the western cordillera. It seems therefore that the IVC developed upon the limit between two major tectonic provinces known to exist at depth. Previous K-Ar dating suggests that the onset of volcanism in the Imbabura complex began around 3.8 Ma at Imbabura and 2.6 Ma at Cubilche (Barberi et al., 1988).

The main Taita edifice is constructed of andesitic lava successions many hundreds of meters thick that are steeply inclined away from Taita summit in all directions. In general the lavas belong to a medium-K magmatic suite and range from low silica andesites to dacites (54% to 64% SiO_2, Fig. 4). Plagioclase, ortho- and clinopyroxene, amphibole, oxides, and accessory olivine are the common minerals. IVC compositions share affinities with lavas of other large edifices of the Ecuadorian volcanic front (Hall and Beate, 1991; Ruiz, 2003; Hall et al., 2008). The IVC suffered at least two major flank failure events; of the resulting debris avalanche deposits the younger is found along the entire NW perimeter of the edifice and traveled up to 17 km away, while the older one was directed toward the present city of Ibarra and traveled 18 km down valley (Fig. 2). Many small hills in the Iluman-Atuntaqui area are ancient hummocks seated upon the main debris avalanche fan and now covered by Cangahua layers. The structural scars resulting from the flank collapses have been largely erased and covered by erosion and younger volcanic activity. The ages of these collapse events remain poorly constrained; they are older than the youngest pyroclastic flow deposits belonging to Mojanda Fuya-Fuya volcano, which have been ^{14}C dated at>43.5

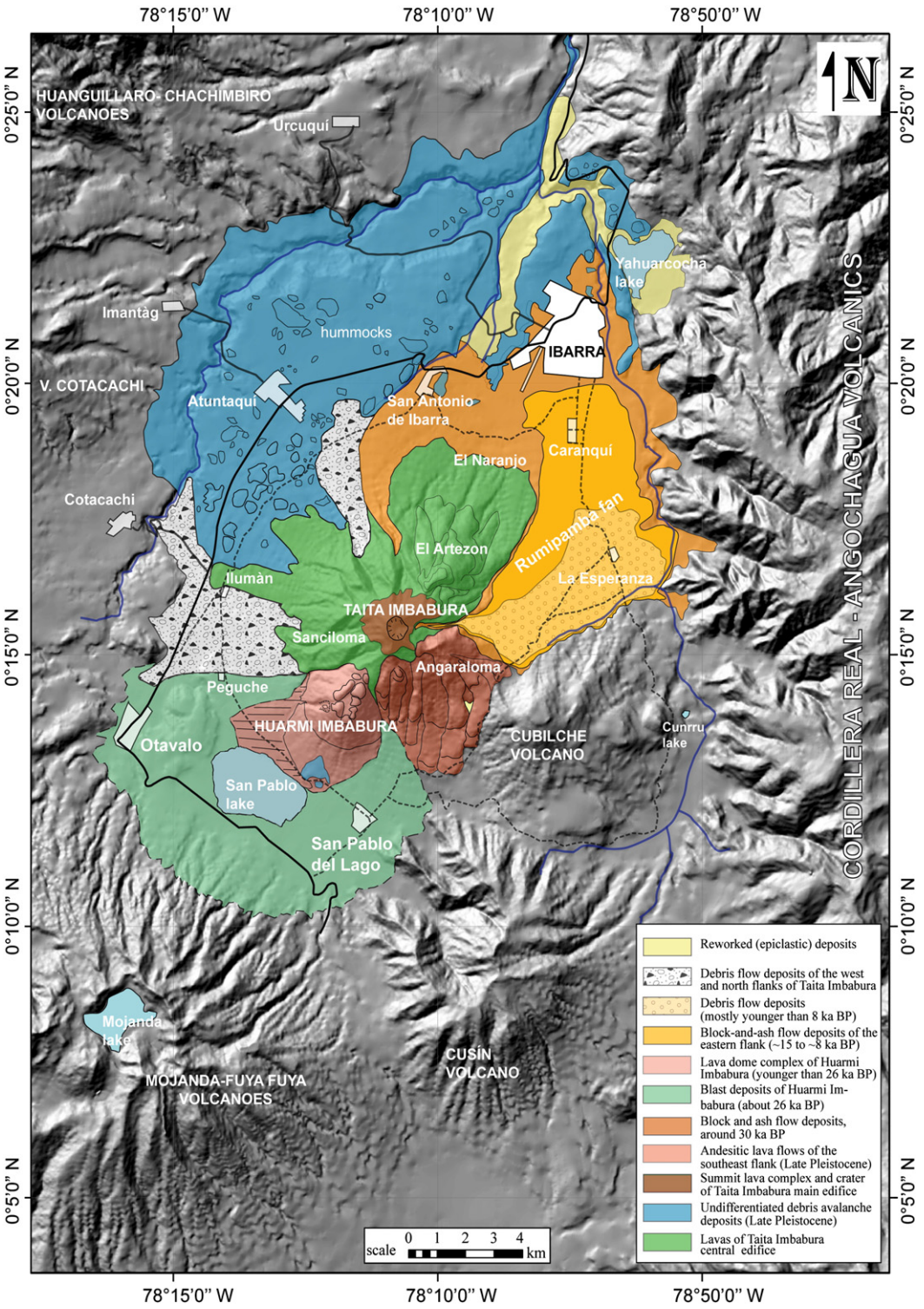

Fig. 2. Simplified geological map of the Imbabura Volcanic Complex (modified after Ruiz, 2003). Heavy and dotted lines are major and secondary roads, respectively. Open areas are towns.

(Robin et al., 1997) and 43.4 ± 2.1 ka BP (this study, Table 1). The presence of ~5–15 m-thick Cangahua deposits on top of the debris avalanche deposits also implies a Pleistocene age.

3. Methods

Our studies at Imbabura were performed during several field seasons from 2000 to 2005. Stratigraphic sections and rock samples were collected all around the edifice, but the paucity of key exposures and the lack of datable material make stratigraphic, chronological and palaeo-morphological evolutions difficult to reconstruct. The selected sections and results presented here focus on the Late Pleistocene to Holocene history and on some geomorphologic features of the volcanic complex. Several rock samples were selected for ^{39}Ar–^{40}Ar age determination. Phenocryst-free whole rock fragments of about 200 mg where irradiated for an hour with cadmium shielding in the McMaster Nuclear Reactor, Ontario, Canada. Samples were processed at the Geochronology Laboratory of Géoazur, University of Nice,


a
Taita Imbabura
47 ± 6 ka
Huarmi Imbabura
7950 ± 150 BP
Lake San Pablo
NW
NE
b
30170 ± 250 BP
Tahuando river
c
d
organic soil
1820 ± 160 BP
2880 ± 100 BP
Pyroclastic flow layer
e
Pyroclastic flow layer
8050 ± 90 BP
Yanahuaycu river bed
f
g

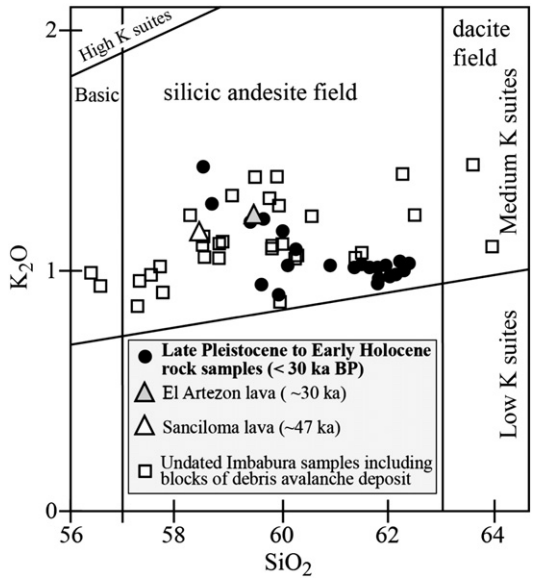

Fig. 4. Plot of K_2O *vs.* SiO_2 for Imbabura rock samples based on major element analyses recalculated to wt. % on an anhydrous base. The Late Pleistocene to Early Holocene rock samples are highlighted with specific symbols in the silicic andesite field of the medium-K magmatic suite of Imbabura. ICP-AES analyses carried out by J. Cotten, Université de Bretagne Occidentale, France.

France with high-frequency furnace heating procedures using experimental techniques described in Féraud et al. (1982). Both plateau and inverse isochron ages were calculated, and preferred plateau ages are given in Table 1. Criteria used to define a plateau age include: 1) at least 60% of total ^{39}Ar is released in the plateau; 2) at least three successive step-heating fractions are analyzed in the plateau; 3) the weighted average of apparent ages for individual fractions concur with each apparent age of the plateau at the 2 σ confidence level.

The radiocarbon data were obtained on charcoal in pyroclastic flow deposits and organic fractions extracted from palaeosoils (Table 1). Most samples were washed with acid to remove possible carbonate and humic contaminants, and a few required the so-called acid/alkali/acid (AAA in Table 1) triple pre-treatment to isolate the datable fraction. The age determinations were performed at the Center for Isotope Research (CIO), Gröningen University, The Netherlands. Large samples were analyzed using the Proportional Gas Counting technique (PGC) while small samples were dated using the Acceleration Mass Spectrometer (AMS) facility at CIO. Conversion of ^{14}C age determinations to calendar ages are based on the Northern Hemisphere atmospheric database of the Intcal09 curve (Reimer et al., 2009) using the Calib 6.0 program (Stuiver and Reimer, 1993; Stuiver et al., 2005). In Table 1 the conventional ^{14}C results are corrected for ^{13}C fractionation and quoted BP (i.e. ^{14}C years before AD 1950) while calibrated ages appear cal BP. All calibrated ages are given as the envelope of the 2-σ age range cal BP and are rounded off to nearest significant 10 years. Major and trace element concentrations were measured on whole rock samples by ICP-AES at the "Laboratoire des Domaines Océaniques" at Brest University, France. Here, selected analyses are presented (Table 2) to highlight the magmatic compositions of late Pleistocene to early Holocene activity, in comparison with the composition of older lavas.

4. Evidence for activity in late Pleistocene to early Holocene times

4.1. Age constraints inferred from geomorphological features and Ar–Ar data

Quaternary studies in the Northern Andes have recognized many glacial advances and retreats, most notably the Late Glacial Maximum (LGM) glaciation (~33–14 ka BP) and evidence of widespread glaciations is very common at most Pleistocene volcanoes in Ecuador. The Younger Dryas (YD) glaciation (12–10 ka BP) has been identified in the Ecuadorian cordilleras (Clapperton, 1993b; Clapperton et al., 1997; Rodbell and Seltzer, 2000), in Colombia (Thouret et al., 1996) and Venezuela (Mahaney et al., 2008). Cirques and U-shaped valleys are typical of the glacial erosion that repeatedly affected this region (Clapperton, 1990, 1993a; Thouret, 1999). Such erosion has also modified many volcanic structures and removed most fragmental deposits older than about 13 ka BP above ~3800 m asl and above 3500 m asl in glacial valleys.

The higher elevations of Imbabura volcano display both depositional and erosional glacial features. Sets of two parallel ridges are found at 3300–3400 m asl near the SW foot of Taita and at 3600 m to the S of Taita's summit, both of which must be glacial moraines given their setting and morphology; their elevations suggest that they belong to the LGM glaciation. In nearby volcanoes YD terminal moraines are found at 3800–4000 m asl elevations. The headwaters of several ravines around Taita's summit form small circular basins, akin to YD glacial cirques, and the presence of glacial-like striations above 4000 m asl would corroborate this interpretation. In summary the higher elevations of Taita suffered glaciations of both LGM and YD periods.

However, a few geomorphological features suggest that volcanic activity took place after the last LGM events at ~14 ka BP. The east side of Taita volcano has a large, eastward-dipping apron of only partially consolidated pyroclastic breccias (herein called the "Rumipamba fan") which are incised by several gullies radiating from the summit area. The apex of the fan above 3800 m shows no evidence of glacial reworking, although it should be expected if emplaced during the LMG period, as glacial advances were more pronounced on the Eastern side down to 3100 m asl.

The western side of Taita Imbabura is incised by steep-sided, ~1000-m-deep gorges which expose thick lava successions. At Sanciloma (Fig. 2), a sample from the uppermost lavas yielded a ^{39}Ar–^{40}Ar isochron age of 47 ± 6 ka (Figs. 3a, 5 and 6, Table 1), implying that the steeply inclined ramparts of the edifice are at least this age and that the gorges were probably carved during LGM times between 33 and 14 ka (Clapperton, 1993a; Clapperton et al., 1997). The satellite peak known as El Artezon, also comprised of andesitic lavas, has a youthful perspective. Compared to other Pleistocene volcanic edifices of the same elevation in Ecuador's eastern cordillera, the summit of El Artezon seems only moderately eroded. A sample from its upper lava sequence yielded a whole rock ^{39}Ar–^{40}Ar isochron age of 30 ± 4 ka (Figs. 5 and 6, Table 1), which coincides with the last major glacial advance in Ecuador (Clapperton et al., 1997). It suggests that the El Artezon edifice was still active in LGM times, and possibly continued into YD times as evidenced by a lack of notable glacial erosion. Both the Sanciloma and El Artezon lavas have andesitic compositions typical of the medium K suite of the Imbabura complex (Fig. 4, Table 2), supporting a common magma source at depth, and not autonomous volcanic systems.

Fig. 3. (a) View of SW side of Imbabura volcano (Taita and Huarmi centers). Locations of two dated samples are indicated. (b) A ~40 m-thick section in block-and-ash flow deposits near the Tahuando River (cow for scale inside the circle). (c) Coarse-grained surge deposits in the Rumipamba pyroclastic fan, E of Taita center. (d) Upper section of the Yanahuaycu ravine, near Cubilche volcano, showing the stratigraphic position of dated andisols. (e) View of the Yanahuaycu ravine and the pyroclastic flow section with interbedded early Holocene andisols. (f) A clastic dike below the blast deposit W of lake San Pablo. Scale is 30 cm. (g) Closeup view of the blast deposit showing the coarse-grained, fines-free matrix, and the angular, breadcrust and radially-jointed juvenile clasts.

Table 1
Radiometric results for Imbabura volcano from this study and previous works. (a) Pretreatment methods to remove contaminants from samples include acid washing (A) and acid/alkali/acid cleaning (AAA). (b) The calendar conversion was obtained using Calib 6.0 (Stuiver et al., 2005), with the Intcal09 calibration curve (Reimer et al., 2009). Calibrated date ranges are the envelope of results obtained at the 2 σ confidence level and are rounded to the nearest significant 10 years. Data with asymmetric standard deviation were calibrated using the largest error value.

Lab. code	Locality	Type of deposit	Type of sample (pretreatment)[a]	UTM coordinates (easting/northing)	^{14}C age (years BP)	±1σ error	δ^{13}C (‰)	Calendar age range (cal BP) (2-σ confidence level)[b]	Reference
GrN-26555	Yanahuaycu ravine	Soil	soil (A)	818220/27413	1820	160	−24.27	1380–2130	This study
GrA-28328	El Naranjo	Soil	Soil, alcali extract (AAA)	819238/32608	1990	35	−18.22	1860–2040	This study
GrN-26556	Yanahuaycu ravine	Soil	Soil (A)	818234/27412	2880	100	−22.91	2780–3320	This study
GrN-27483	Cerro El Araque	Soil	soil (A)	811426/24238	7940	150	−18.87	8420–9250	This study
GrN-27017	Yanahuaycu ravine	Soil	Soil (A)	820568/28742	8050	90	−21.75	8630–9250	This study
Beta	El Naranjo area	Pyroclastic flow dep.	Charcoal	819200/32200	14310	300	-	16,800–18,440	Hall and Beate (1991)
GrN-28892	NE flank of Mojanda volcano	Blast layer	Charcoal (A)	810273/19620	24970	+310/−300	−23.29	29,220–30,470	This study
GrA-34137	N flank of Cusin volc.	Blast layer	Charcoal (AAA)	812961/19828	26930	+170/−160	−23.72	31,070–31,490	This study
GrN-27484	Summit area of Coritola hill	Coarse-grained ash layer	Charcoal (A)	807488/26014	28050	+820/−750	−24.10	31,190–34,450	This study
Beta-60549	Tahuando river	Pyroclastic flow dep.	Charcoal		30000	310	-	33,800–35,160	Hall and Beate (1991)
GrN-29301	Tahuando river	Pyroclastic flow dep.	Charcoal (AAA)		30170	250	−22.04	34,470–35,200	This study
Obdy-1318	Chozon area, Mojanda volcano	Pyroclastic flow dep.	Charcoal	801390/21437	>35000		-		Robin et al. (1997)
GrN-28893	Coritola hill	Coarse-grained ash layer	Charcoal (A)	807488/26014	>38000		−22.23		This study
GrN-26586	Road cut near Peguche	Pyroclastic flow dep.	Charcoal (A)	807400/27300	43400	+2100/−1600	−24.93	45090–48670 (at 1-σlevel) 43970–[50000] (at 2 σ level)	This study
GrN-22435	Cochasqui (Mojanda volc.)	Pyroclastic flow dep.	Charcoal (A)	?	>43500		−24.16		Robin et al. (1997)
Lab. code	Locality	Type of rock	Type of sample	Isochrone age (ka ± 2 sigma)	MSWD	(^{40}Ar/^{36}Ar)i	Plateau age (ka ± 2 sigma)	Steps in plateau vs total steps (and % ^{39}Ar included)	Reference
M2049 (IM62)	East flank of El Artezon	Andesitic lava	whole rock (227 mg)	30 ± 4	0.4	295 ± 2.2	30 ± 4	5 to 10/14 (75% 39Ar)	This study
M2048 (IM57)	Western flank of Taita cone	Andesitic lava	whole rock (211 mg)	47 ± 6	0.9	295 ± 1	47 ± 6	5 to 9/14 (76% ^{39}Ar)	This study

The S and SE flanks of Taita are covered by thick lava flows with almost pristine morphologies (Angaraloma area in Figs. 2 and 5). Lateral levees, bulging flow fronts, and obvious ogive structures within the lava channels are still recognizable in the flows as high as 3800–3900 m elevation. The absence of marked glacial erosion of these flows at such high elevations suggests that these lavas were emplaced at the end of or after the LGM period, e.g. after about 18–14 ka BP. Notably, our attempt to date these lavas with ^{39}Ar–^{40}Ar techniques failed because of the high content of atmospheric argon trapped in the samples, compared to the low production of radiogenic isotopes, consistent with an age younger than ~30 ka.

4.2. Evidence of magmatic activity from radiocarbon dating

The Rumipamba fan on the eastern flank of the Taita complex is a large and gently inclined apron composed of pyroclastic and debris flow deposits, now incised by narrow gullies and ravines. The deposits can be traced upward to 3800 m asl, converging to a source in the eroded crater of Taita Imbabura. Where exposed, the deposits show no clear evidence of glacial reworking. They mostly consist of monotonous block-and-ash flow units, in which each unit is ~2–5 m thick. Their total accumulation locally reaches 30–50 m, e.g. near the Tahuando River (Fig. 3b), and more than 80 m near the apex of the Rumipamba apron. Wavy stratified surge deposits are also exposed (Fig. 3c) and probably represent the overbank or frontal facies of the clast-supported block-and-ash flow units. A whitish to pinkish fine-grained ash matrix between the clasts is observed at many localities, while matrix-free, clast-supported deposits are also common. The juvenile fraction commonly makes up more than ~95 vol% of the deposit and consists of light-toned subangular to slightly rounded, poor to moderately vesiculated blocks, a few cm to 20–40 cm in diameter. These clasts are medium K silicic andesites to low silica dacites, with 59.6–62.3% SiO_2, 3.5–3.9% Na_2O, 0.9–1.2% K_2O (Table 2). Xenoclastic material (old lava clasts) amounts to less than 5 vol% of the deposits.

In the Tahuando River section (Fig. 3b) the exposed lowermost unit contains more vesiculated pumiceous bombs, as well as carbonized trunks and branches which have been ^{14}C dated at 30,000 ± 310 BP (Hall and Beate, 1991). A ^{14}C age of 30,170 ± 250 BP (GrN-29301) obtained in this work concurs with the above result, and both point to calendar ages in the range of 33.8–35.2 ka cal BP (Table 1). These lower units therefore mark the onset of a period of major pyroclastic flow activity erupted from Taita Imbabura's summit. Similar block-and-flow deposits exposed in El Naranjo area on the N side of the volcano hosted charcoal which yielded an age of 14,310 ± 300 BP (Hall and Beate, 1991), revealing that eruptive activity was also taking place around 16.8–18.5 ka cal BP, i.e. in late LGM times (Clapperton et al., 1997). The base of the dark palaeosoil which caps the pyroclastic flow deposits in the El Naranjo area is AMS-dated in this work at 1990 ± 35 BP (GrA-28328; Table 1), corresponding to a calendar interval of 1.86–2.04 ka cal BP at the 2-σ confidence level. This age is much younger than the last pyroclastic flows of the El Naranjo area, but may serve as a limiting age for the youngest units.

The Punguhuaycu ravine separates Imbabura and Cubilche volcanoes and continues upstream to the Yanahuaycu gully on Taita Imbabura (Fig. 2). Similar block-and-ash flow units are exposed there (Fig. 3d and Sections 1 and 2 in Fig. 7), lying upon post-avalanche lavas belonging to nearby Cubilche volcano (Fig. 2). An interbedded dark palaeosoil horizon, which denotes a pause in the accumulation of these flow units, yielded a ^{14}C age of 8050 ± 90 BP (GrN-27017; Fig. 3e, Table 1). At the 2-σ confidence level the calibrated ages are in the range 8.63–9.25 ka cal BP. The overlying block-and-ash flow deposit is thus younger.

The reliability of this Holocene age needs to be appraised in the context of a tropical environment. Radiocarbon dating results in the Ecuadorian Andes highlight occasional discrepancies between the age

of charcoal in palaeosoils and overlying pyroclastic rocks. In the most common cases the ^{14}C age of the underlying soil is younger than that of the pyroclastic deposit, as is documented for example at Pichincha and Chimborazo volcanoes (Barba et al., 2008; Robin et al., 2008, 2010). Such discrepancies may result from contamination by young carbon and humic acids, as evidenced in andisol of northern Ecuador by Tonneijck et al. (2006). Yet, in the above documented examples the maximum age difference is on the order of a few hundreds of ^{14}C years. If the age of the palaeosoil in the Punguhuaycu ravine is also slightly rejuvenated, the age of the overlying pyroclastic flow deposits would be younger than ~9.0–9.7 ka cal BP, corresponding to early Holocene times.

Higher in the ravine, near the western rampart of the El Cubilche collapse scar (Fig. 5), the uppermost block-and-ash flow deposits are covered by palaeosoil horizons interbedded with overbank debris flow layers (Fig. 3d). The lower palaeosoil is dated at 2880 ± 100 BP (GrN-26556), while the upper horizon yields an age of 1820 ± 160 BP (GrN-26555). These ages translate into calendar intervals of 2780–3320 cal BP and 1380–2130 cal BP, respectively (Table 1). These results argue for intense erosional activity in the first millennium BC with concomitant debris flows which presumably impacted fluvial terraces along the Tahuando River, as well as limiting the age of the block-and-ash flow activity.

4.3. A major late Pleistocene volcanic blast event from Huarmi Imbabura

The top of Coritola hill N of Lake San Pablo exposes a succession of Cangahua and pyroclastic units (Fig. 5 and Section 3 in Fig. 7). Conspicuous pyroclastic breccias are exposed beneath the uppermost 2.5 m of soil interbedded with eolian deposits and these correlate with a widespread volcanic unit described below. Lower in the section a series of ash beds overlies a lithic-rich surge deposit, whose fine-grained base contains charcoal that is dated at 28,050 + 820/−750 BP (GrN-27484) resulting in calibrated ages in the range of 31.19–34.45 ka cal BP (Table 1). Charcoal from a deeper surge layer in the section yielded an age greater than 38,000 BP, i.e. older than 40 ka cal BP.

The upper pyroclastic breccias can be traced laterally on the W, SW and S of the Huarmi dome complex, and it covers a reconstructed surface area of at least 100 km². The deposit shows no stratification and is coarse-grained (Fig. 3g), poorly sorted and in most places massive (some double grading has been observed at several sites). The lack of an interstitial matrix between the clasts is a prominent feature of this unit (Fig. 3g) and imbrication of tabular and elongated blocks has been observed at some sites. At many localities a 10–40 cm-thick, whitish to pinkish, fine-grained and massive ash layer occurs at the base of the deposit. The juvenile blocks in the main layer are poorly vesiculated, relatively dense angular to sub-angular clasts, and partially bread-crusted surfaces and radial cooling joints in the clasts are common features. Silicic andesites (61–62% SiO_2, Table 2) containing plagioclase, ortho- and clinopyroxene, amphibole, oxide minerals and glass dominate. A charred twig collected within the layer on the eastern flank of Mojanda (Fig. 5) yielded a PGC radiocarbon age of 24,970 + 310/−300 BP (GrN-28892; Table 1), while small crushed charcoal debris on the northern flank of Cusín volcano, S of Imbabura, yielded an AMS age of 26,930 + 170/−160 BP (GrA-34137). When calibrated, these ages convert to 29.2–31.5 ka cal BP (Table 1).

Isopach and isopleth maps, along with field observations indicate that this pyroclastic breccia blanketed the pre-eruptive topography and originated from a source on the SW side of IVC (Fig. 8). The measured thickness of the layer decreases from 120 cm on top of El Araque hill to less than 10 cm on the eastern slopes of Mojanda volcano (Fig. 8a), but it correlates with distance only beyond ~8 km from the source, and with elevation only above ~2900 m asl on Mojanda's flank (dotted lines in Fig. 9a and b, respectively). Consistently, the deposit is coarser-grained on the top of El Araque hill, where the average length of the five largest xenoclastic blocks exceeds 70 cm and decreases to less than 10 cm to the W and S (Fig. 8b).

We interpret this breccia as a volcanic blast erupted from a vent now concealed beneath Huarmi Imbabura, a large lava dome complex located on the southwestern flank of the Taita Imbabura edifice. The dome complex grew within the blast crater carved in the 20–25° inclined slopes of Taita's flank. Our study shows that the crater formed during a catastrophic explosive event that generated a debris avalanche and a powerful directed blast which spread westward. The only outcrop of the avalanche deposits is exposed as a pyramid-shaped hummock known as El Araque hill (located in Fig. 5), preserved at the SW base of IVC. We assume that most of the debris avalanche deposit filled the valley and is now masked beneath Lake San Pablo. On the top of El Araque hill the debris avalanche deposits are overlain directly by volcanic breccias of the blast deposit, evidencing their origin during the same explosive event.

4.4. Clastic dikes that underlie the blast deposit

The blast deposit is underlain by a remarkable set of clastic dikes that penetrate into the substrate beneath the unit down to 3–5 m (bottom end is rarely observable and propagation of the cracks above the blast deposit has been observed nowhere). These fractures are observed in a limited area at the western periphery of Lake San Pablo and their areal distribution decreases rapidly on the slopes of Mojanda. The dikes consist of sub-vertical or steeply inclined opened fractures filled with clastic materials that are similar to that of the blast deposits in terms of components, grainsize, and texture (Fig. 3f). Some exposures show that many fractures narrow uniformly with depth, and where observable, the dikes are connected to the blast deposit with no visible discontinuity, as if the blast deposit was the source material which filled up the dikes during or soon after deposition. To gain insight into the origin of these dikes we measured the width and orientation of 43 dikes in the area W of Lake San Pablo. Results show that the fractures are typically 2 to 25 cm wide, with a regular decrease of dyke width frequency with fracture size in the investigated area (Fig. 10a), and that the studied dike population displays no clearly preferred azimuthal orientation (Fig. 10b), suggesting little or no tectonic control of their formation. Their possible origin is discussed below.

5. Magmatic budget

To appraise the importance of the volcanic activity at Imbabura, we evaluated the minimum volume of the erupted products emplaced from 35 ka cal BP to the present. Estimating the size of ancient effusive and pyroclastic eruptions is a difficult task at Imbabura because of erosion and lack of exposures. In this work we combined our geological observations with the examination of topographic maps, aerial photos and satellite images and thereby measured minimum lengths and widths of post-35 ka cal BP volcanic units. Thicknesses were estimated during field work. We consider that these volumetric estimates and age constraints are reliable enough to obtain a relevant value of the *minimum* magma output rate for the above time interval. This magma volume is expressed here as Dense Rock Equivalent (DRE), after discarding the xenolithic fraction disseminated in the pyroclastic deposits and converting to non-porous magmatic rocks.

The Rumipamba pyroclastic fan on the eastern flank of Imbabura can be described as a sector of a flat cone which gently dips northeastward to the Tahuando River. The height of the hypothetical cone is set at 100 m (the deepest gullies of the Rumipamba fan expose ~80 m thick deposits), which thins to 0 m at 8 km downslope to the Tahuando River. By considering that the fan represents one third of the cone, we obtain a bulk volume of 2.23×10^9 m^3. Removing 5% of the xenoclastic material and assuming a bulk porosity of 30% (20% for

Table 2
Whole rock analyses of Late Pleistocene to Early Holocene volcanic rocks from Imbabura volcano. Major (in wt.%) and trace (in ppm) elements analyses were obtained at the Université de Bretagne Occidentale, Brest, (UBO, France). Agate-ground powders were analyzed by ICP-AES, except for Rb, which was measured by atomic absorption analysis. Relative standard deviation is 1% for SiO_2 and 2% for other major elements.

Location	Taita Imbabura	El Artezon	Rumipamba pyroclastic fans							Ibarra area				
Local place name	Southwest flank	East flank	El Naranjo		Rumitola	Zapallo Loma	Cachaloma			Imbaya	Pucara Alto	East Ibarra		
Rock type	Lava flow	Lava fow	Juvenile blocks in pyroclastic flow deposits							Juvenile blocks in pyroclastic flow deposits				
Sample #	CIM-57	CIM-62	CIM-22	CIM-33	CIM-34	IMB-4	CIM-42	CIM-43	CIM-44	IMB-11	CIM-12	IMB-14	IMB-45	IMB-16
UTM-X (m)	107	168	197	220	058	178	173	173	179	177	111	227	227	226
UTM-Y (m)	284	297	323	295	236	276	339	339	340	422	342	375	335	370
SiO_2	58.46	59.55	59.95	61.70	62.26	59.63	60.04	60.27	59.64	59.44	58.71	61.37	61.65	61.70
TiO_2	0.62	0.60	0.53	0.49	0.46	0.53	0.57	0.53	0.59	0.59	0.61	0.48	0.48	0.48
Al_2O_3	17.11	17.40	17.75	17.76	17.68	17.65	17.49	17.67	17.85	17.15	17.82	17.55	17.41	17.26
Fe_2O_3*	7.37	6.90	6.81	6.04	5.79	6.75	6.72	6.65	6.75	6.73	6.98	5.86	5.87	5.95
MnO	0.11	0.12	0.13	0.12	0.12	0.12	0.12	0.12	0.12	0.12	0.12	0.11	0.11	0.11
MgO	4.31	3.39	2.90	2.44	2.28	3.13	3.27	3.05	3.17	3.59	3.56	2.61	2.57	2.58
CaO	7.10	6.84	7.20	6.49	6.35	7.53	6.82	6.73	6.84	7.48	7.07	7.00	6.87	6.92
Na_2O	3.62	3.72	3.61	3.75	3.84	3.49	3.60	3.69	3.60	3.47	3.64	3.79	3.82	3.79
K_2O	1.16	1.22	0.90	1.00	1.01	0.93	1.16	1.08	1.21	1.20	1.28	1.01	1.01	1.01
P_2O_5	0.14	0.25	0.21	0.20	0.20	0.22	0.21	0.21	0.23	0.23	0.21	0.22	0.20	0.20
TOTAL	100	100	100	100	100	100	100	100	100	100	100	100	100	100
LOI	-0.09	0.16	0.7	1.57	0.32	0.57	0.57	0.77	1.64	0.44	0.92	0.34	0.91	0.88
Rb	23	19	14.5	16.5	16.8	17	19.2	17.7	20.5	30	21	23	15	16
Sr	615	1065	800	735	750	781	960	905	1010	986	1064	740	742	748
Ba	575	850	465	505	520	443	682	590	785	708	775	492	494	498
Sc	22	16.7	13	12	11	16.2	15	16	17.7					
V	186	185	135	116	108	140	125	132	153					
Cr	64	23	12	13	9.5	22	19	18	22	31	17	15	18	23
Co	24	18	16	14	12	17	16.5	18	19					
Ni	41	18	10	9	7	6	16	15	17	10	19	5	4	3
Y	15	16.5	16	14.4	14.5	16.5	15	16	18.2					
Zr	82	95	86	92	92	58	91	85	98	39	90	79	60	70
Nb	2.8	3.7	3.3	3.2	3.1	3	3.2	3.6	3.4					
La	9.2	23	13.5	13	14.5	20	16.7	22.5	18.8					
Ce	19.5	43	26.5	26	27.5	38	33	42	34.5					
Nd	10.8	21.5	14	14.5	14.5	19.5	16.5	21.5	18.5					
Sm	2.55	3.9	3.15	3.1	2.9	3.5	3.2	4.1	3.75					
Eu	0.84	1.15	0.93	0.85	0.88	1.06	0.96	1.12	1.09					
Gd	2.75	3.4	2.9	2.6	2.7	2.9	2.9	3.4	3.25					
Dy	2.4	2.65	2.6	2.3	2.5	2.7	2.5	2.75	2.9					
Er	1.45	1.6	1.5	1.4	1.55	1.6	1.5	1.7	1.8					
Yb	1.44	1.56	1.48	1.35	1.44	1.58	1.44	1.55	1.8					
Th	2.6	8.3	3.25	3	3.5	7	5.2	8.2	7.4					

Location	Tahuando river					Huarmi Imbabura								
Local place name	East Ibarra	East Caranqui		La Josefina	La Esperanza	Summit domes						Quebrada Azaya		Calpaqui
Rock type	Juvenile blocks in pyroclastic flow deposits					Lava dome blocks								
Sample #	CIM-11	CIM-35	CIM-36	CIM-39	CIM-56	CIM-15	CIM-16	CIM-17	CIM-18	CIM-19	CIM-20	CIM-24	CIM-26	CIM-45
UTM-X (m)	217	231	231	172	236	126	124	126	126	125	126	192	115	058
UTM-Y (m)	385	355	355	325	325	259	261	261	262	259	258	263	263	236
SiO_2	61.95	61.80	61.83	60.13	62.04	60.92	61.79	61.59	62.34	62.22	61.50	62.10	62.01	62.25
TiO_2	0.48	0.48	0.47	0.54	0.48	0.49	0.48	0.48	0.50	0.45	0.49	0.44	0.48	0.47
Al_2O_3	17.51	17.61	17.76	17.73	17.60	17.65	17.65	17.55	17.81	17.62	17.71	17.70	17.60	17.45
Fe_2O_3*	6.01	6.10	6.00	6.69	5.81	6.19	6.08	5.96	6.21	5.68	6.13	5.66	5.86	5.99
MnO	0.11	0.12	0.12	0.13	0.12	0.11	0.11	0.11	0.11	0.11	0.11	0.11	0.12	0.12
MgO	2.43	2.45	2.42	3.05	2.44	2.45	2.43	2.38	2.47	2.47	2.50	2.38	2.35	2.33
CaO	6.46	6.41	6.34	6.92	6.54	7.06	6.33	6.85	6.43	6.39	6.43	6.57	6.50	6.40
Na_2O	3.84	3.89	3.87	3.59	3.78	3.88	3.92	3.88	2.90	3.82	3.91	3.86	3.90	3.78
K_2O	1.02	0.95	0.97	1.02	0.98	1.02	1.01	1.01	1.03	1.04	1.02	0.98	0.98	1.00
P_2O_5	0.19	0.19	0.20	0.20	0.21	0.22	0.19	0.19	0.19	0.20	0.19	0.19	0.19	0.20
TOTAL	100	100	100	100	100	100	100	100	100	100	100	100	100	100
LOI	1.11	0.33	1.01	0.95	0.99	0.69	0.27	0.97	0.18	0.92	0.17	0.38	0.13	0.28
Rb	17	17	17	16.7	15.5	16.5	18	18	17.2	18	17.2	17	17.8	17
Sr	737	746	740	910	765	717	702	700	698	690	712	733	740	745
Ba	505	500	496	574	500	530	530	535	535	535	522	501	505	512
Sc	11.4	11.7	11.2	14.6	11.4	12	12	11.6	12	11.6	12	11.3	11.6	11.5
V	118	114	113	123	112	136	126	114	123	108	124	102	147	112
Cr	11	15	12.5	16.5	14	9	9	13	11	10	10	12	11	11
Co	16	12.5	14	16.5	15	14	14	13.5	14	13.5	14	12.5	12.5	13
Ni	13	9.5	10	14	11	9	9	9.5	9	9	9	8	8.5	8
Y	14.3	14.6	13.8	15	14.5	14.3	13.8	14.1	14.3	14.3	14.5	15	15	14.8
Zr	90	91	89	86	88	91	90	90	92	90	92	92	96	93
Nb	3.2	3	3.1	3.2	3.1	3	3.1	3	3	3	3	3.2	3	3
La	13.6	14.7	13.8	16.8	13.5	11.5	10.8	12.2	11.8	11.5	12.1	12.3	12.5	14
Ce	26	28	27.5	30.5	26	23	21.5	25	23	24	23	24.5	26	26.5
Nd	14.8	15	14.5	16.5	14.8	13	12.6	13.6	13.6	13	13.6	14	14	15
Sm	2.85	2.8	2.7	3	3.15	2.85	2.7	2.75	2.8	2.7	2.85	2.85	2.9	3.05
Eu	0.86	0.89	0.85	0.95	0.9	0.84	0.87	0.83	0.85	0.84	0.87	0.86	0.86	0.89
Gd	2.65	2.4	2.4	2.8	2.75	2.55	2.25	2.55	2.5	2.6	2.5	2.7	2.5	2.7
Dy	2.3	2.35	2.3	2.5	2.5	2.25	2.2	2.25	2.3	2.35	2.3	2.35	2.45	2.4
Er	1.35	1.5	1.4	1.45	1.45	1.4	1.35	1.35	1.45	1.4	1.45	1.45	1.45	1.45
Yb	1.36	1.42	1.34	1.47	1.42	1.4	1.35	1.35	1.41	1.38	1.4	1.47	1.45	1.46
Th	3.45	3.5	3.25	5.2	3.2	2.65	2.7	2.65	2.75	2.75	2.8	2.95	3.15	3.5

* Total iron as Fe_2O_3.

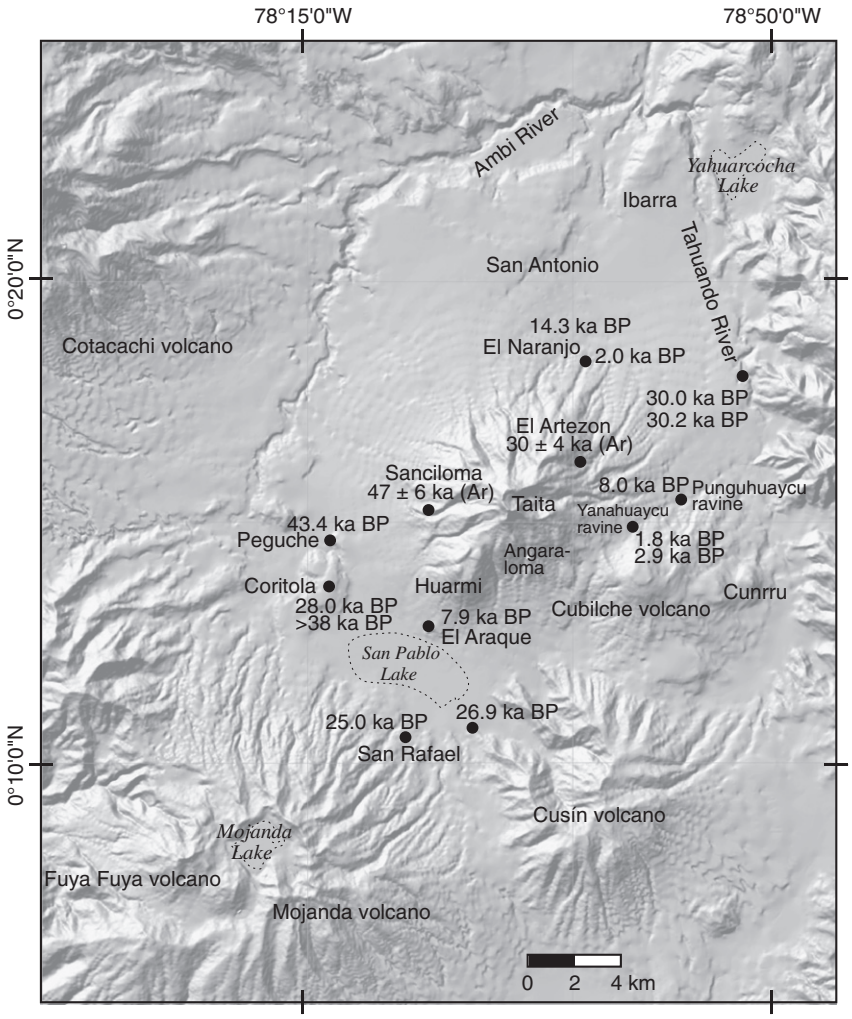

Fig. 5. Map showing the location of the dated samples and sections studied. The Punguhuaycu ravine (Section 1) separates Imbabura and Cubilche volcanoes and continues upstream to the Yanahuaycu gully (Section 2) on Taita Imbabura. Section locality names indicated in Fig. 5.

inter- and 10% for intra-particle void space) yields a DRE volume of 1.45×10^9 m^3. The volume of the deposits at the northern base in El Naranjo and San Antonio areas is much smaller and amounts to ~0.05×10^9 m^3 DRE, after also removing 35% for porous and xenoclastic fractions. In total the minimum DRE volume for the block-and-ash flow deposits of the IVC's eastern and northern sides is thus around 1.5×10^9 m^3.

As indicated above, the blast layer thickness decays away from a source located beneath the Huarmi Imbabura dome complex. A plot of the isopach thickness vs. square root of isopach area reveals that the blast layer thins almost linearly with distance from its source (Fig.10c), but the data fit better ($R^2=0.996$) to a logarithmic law of the form $T=-1.56\times\ln(A^{1/2})+14.43$, where T and A are isopach thickness and area, respectively. Using the trapezoidal rule approximation technique to calculate the volume of tephra fall deposits (Froggatt, 1982; Fierstein and Nathenson, 1992), and neglecting the lost ash-sized fraction and the ballistic component, as well as setting the minimum near-vent thickness at 3 m gives a bulk volume of about 82×10^6 m^3. To convert this bulk volume to DRE we again set the porosity at 30% but removed10% to account for non-juvenile material in the layer, which then yields a dense magma volume of at least 52×10^6 m^3.

The geometry of the post-blast Huarmi dome complex can be simplified to that of a regular truncated cone. We set the base at 3000 m asl (i.e. 100 m above of the top of El Araque hill) and the summit plateau at 3750 m asl, a total cone height of 750 m. The average basal radius is about 1700 m, and the summit radius 550 m, which yields a bulk truncated cone volume of 3.2×10^9 m^3. Assuming a bulk lava dome porosity of 15% (bubbles, fractures, etc.), we obtain a DRE volume of 2.8×10^9 m^3 of silicic andesite for this dome complex. Although the thick pristine lava flows of the southern flank remain undated in this work, we consider that their youthful age is close to that of the block-and-ash deposits. Their volume was estimated from maps and aerial photos, which yielded a minimum bulk volume of 0.28×10^9 m^3, corresponding to 0.22×10^9 m^{3}after removing 20% for porosity. Consequently, the total *minimum* DRE volume emplaced during the past 35 ka cal BP amounts to 4.6×10^9 m^3, which gives an average output rate of at least 0.13×10^9 m^3/ka.

6. Discussion

6.1. Reconstructing late Pleistocene to early Holocene activity

Our geological research at Imbabura volcano reveals that the volcano experienced significant eruptive episodes in late Pleistocene to early Holocene times. ^{39}Ar–^{40}Ar dating indicates that andesitic lavas were still being emplaced at ~47 ka on the upper slopes of Taita Imbabura and were virtually sub-contemporaneous to the last dacitic pumice flow eruptions from nearby Fuya-Fuya volcano, dated at ~44–50 ka cal BP (Robin et al., 1997, 2009). The lavas dated at 30 ka at El Artezon were presumably emplaced during the major LGM advance dated in Ecuador around 30–14 ka BP (Clapperton et al., 1997). The

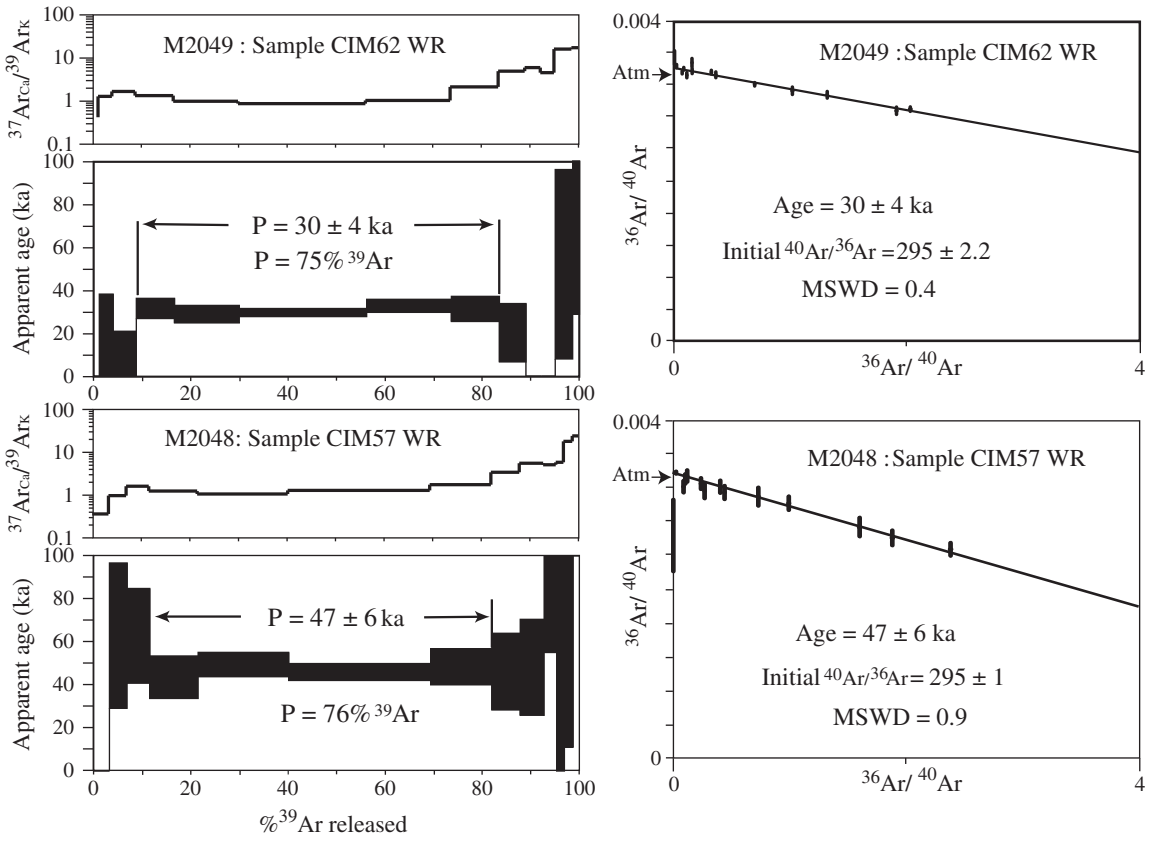

Fig. 6. ^{40}Ar–^{39}Ar age and $^{37}Ar_{Ca}/^{39}Ar_K$ ratio spectra (furnace heating) obtained on whole rock from lava flows of Saciloma (upper) and El Artezon (lower). Plateau ages (P) are given at the two sigma (2σ) uncertainty (Table 1) but thickness of solid rectangles corresponds to 1σ on apparent ages of each individual step. Atm = Atmospheric ratio figured on the inverse isochron diagrams. Ages were calculated from measured isotope ratios corrected for mass discrimination, system blanks, and interfering isotopes produced during irradiation. Correction factors for interfering isotopes are $(^{39}Ar/^{37}Ar)Ca = 0.00073 \pm 4\%$, $(^{36}Ar/^{37}Ar)Ca = 0.00282 \pm 3\%$, and $(40Ar/39Ar)K = 0.001 \pm 3\%$. Age calculations are made using the decay constants of Steiger and Jäger (1977).

age of the early Tahuando pyroclastic flow deposits is analytically indistinguishable from that of the El Artezon lavas. However, field relationships suggest that the Tahuando block-and-ash flow successions were emplaced after the growth of El Artezon. Based on geomorphological evidence we assume that the undated well-preserved lavas of the southern flank were also emplaced during the ~30–20 ka BP period.

Dome growth activity commenced at the Taita summit around 35 ka cal BP, with block-and-ash-flows that traveled more than 10–12 km down the NE slope of Imbabura. Surge layers at Coritola hill dated at around 31.2–34.5 ka cal BP, possibly correlate to this period of intense pyroclastic activity. The flank collapse on IVC's SW side, likely related to Huarmi's incipient dome intrusion was followed by a powerful blast event around 29.2–31.5 ka cal BP. The juvenile clasts in the blast layer have silicic andesite compositions that compare to those of the preceding Taita magmas and later Huarmi dome lavas. Based upon a similar mineralogy and chemical composition, we infer that the Huarmi Imbabura crater may be considered as a lateral vent of the central Taita edifice, and not as a separate volcano. Consistently, we found no evidence of magmatic activity in the summit region of Taita around 25–30 ka cal BP.

The clastic dikes that underlie the blast layer are composed of material belonging to the blast deposit. Because there is no evidence of a time lapse between fracture formation and their filling, we infer that the dikes formed during or soon after the emplacement of the blast deposit. This raises the possibility that the fractures formed by means of an extensional event related to the explosive blast. The fractures may have opened as a consequence of a sudden relaxation of the local stress field associated with the depressurization of the southwestern flank of the Imbabura edifice, thus explaining the lack of tectonic control on clastic dike orientation. The timing of the subsequent Huarmi dome growth episodes remains poorly constrained, but a dated soil overlying dome breccias indicates that the emplacement ended before 8.4–9.3 ka cal BP, after production of more than 2.8 km^3 of homogeneous silicic andesite. The alignment of the Huarmi domes, the main Taita crater and the El Artezon summit along a single lineament (Fig. 2) suggests that these vents developed above a structural discontinuity rooted in the basement, the NE alignment being a common regional trend, and were fed by a common plumbing system.

Continuing summit activity at Taita is indicated by the block-and-ash flows dated around 16.8–18.5 ka cal BP which spilled down the northern slopes of the edifice and were deposited in the El Naranjo area and probably also along the San Antonio gullies. The dated soils above the El Naranjo deposits suggest that the activity ended well before 2 ka cal BP. Contemporaneous activity of the summit dome complex fed other block-and-ash flow units that piled up on the eastern side, thus contributing to the progressive growth of the Rumipamba apron, but their coverage was seemingly smaller than that of the initial flows at ~35 ka cal BP. However, the presence of a dark palaeosoil dated around 8.6–9.3 ka cal BP in the Punguhuaycu ravine means that significant time intervals separated the accumulation of the pyroclastic units at least on the southern side of the apron. The occurrence of this dated soil implies that the overlying pyroclastic flow deposits were emplaced in early Holocene times, while their limited extension suggests modest eruption sizes (Fig. 2). The progressive decrease of the block-and-ash flows' distribution since the onset of the pyroclastic episode at 35 ka cal BP reflects a waning magma input for that eruptive cycle. The morphologic remnants of a ~700-m-wide crater on Taita's summit suggest that

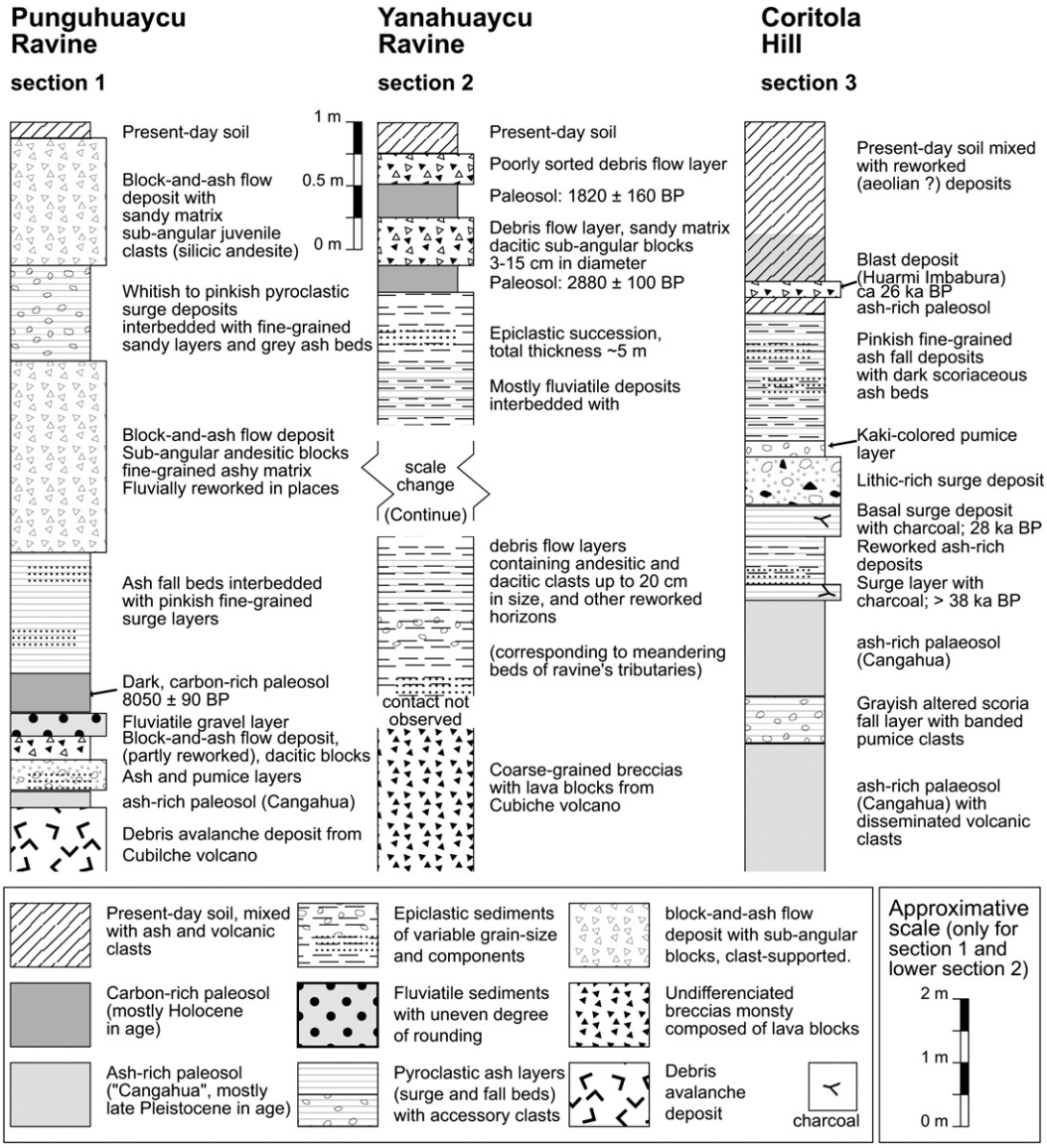

Fig. 7. Selected stratigraphic sections investigated at Imbabura volcano and illustrating Late Pleistocene to Early Holocene deposits on the eastern and western flanks of the edifice. Section sites are located in Fig. 5.

explosive activity continued after its dome-building periods, although the associated pyroclastic products were not identified in this study.

This reconstruction has implications for tephrochronological studies in the Imbabura region. Athens (1999) reported 32 ash horizons interbedded with lacustrine layers in a 14 m-long core drilled in San Pablo Lake, and identified the young 2500 BP Pululahua and the 3000–3100 BP Cuicocha tephra horizons in the ~7 ka cal BP core's record. Based on mineralogical assemblage examination the older tephras were all assigned to Cayambe, which experienced recurrent eruptions in late Pleistocene and Holocene times (Samaniego et al., 1998). Yet, our geological and radiometric findings suggest that renewed examination of these cores is justified to account for possible tephra contributions from Imbabura volcano.

6.2. Implications for hazard assessment

The recent late Pleistocene–early Holocene activity of Imbabura volcano, as reconstructed here, points to a past behavior dominated by eruptions characterized by a low recurrence rate but by rather large sizes. A gross estimate of the volumes erupted in the last 35 ka cal BP points to a minimum magmatic output rate of 0.13 km^3/ka. This rate compares to those inferred for longer time scales at nearby volcanoes in the Ecuadorian arc (e.g. ~0.4 km^3/ka at Cayambe, Samaniego et al., 2005; ~0.3 km^3/ka at Pichincha, Robin et al., 2010), and to those documented at other active volcanoes in a cordilleran setting, such as Mt Adams (0.2–0.4 km^3/ka, Hildreth and Lanphere, 1994), Mt Baker (~0.2–0.3 km^3/ka, Hildreth et al., 2003) and Mt Mazama (~0.4 km^3/ka, Bacon and Lanphere, 2006), all in the Cascade Range, USA. It is also higher than the output rate reported at several active dacitic volcanoes of the Central Andes, e.g. both Ollague (Feeley and Davidson, 1994) and Llullaillaco (Richards and Villeneuve, 2001) are less than 0.1 km^3/ka. In detail this average rate conceals a notable variability in magmatic output at shorter time scales, as observed at other volcanoes of Ecuador's volcanic front, where low recurrence rates correlate with rather high eruption magnitudes (VEI≥4), as reported at Pichincha (Robin et al., 2008,

Fig. 8. Isopach and isopleth maps of the blast deposit emplaced during the collapse of the SW flank of Imbabura volcano, about 30 ka cal BP. MCS is Maximum Clast Size (average length of five largest xenolithic fragments).

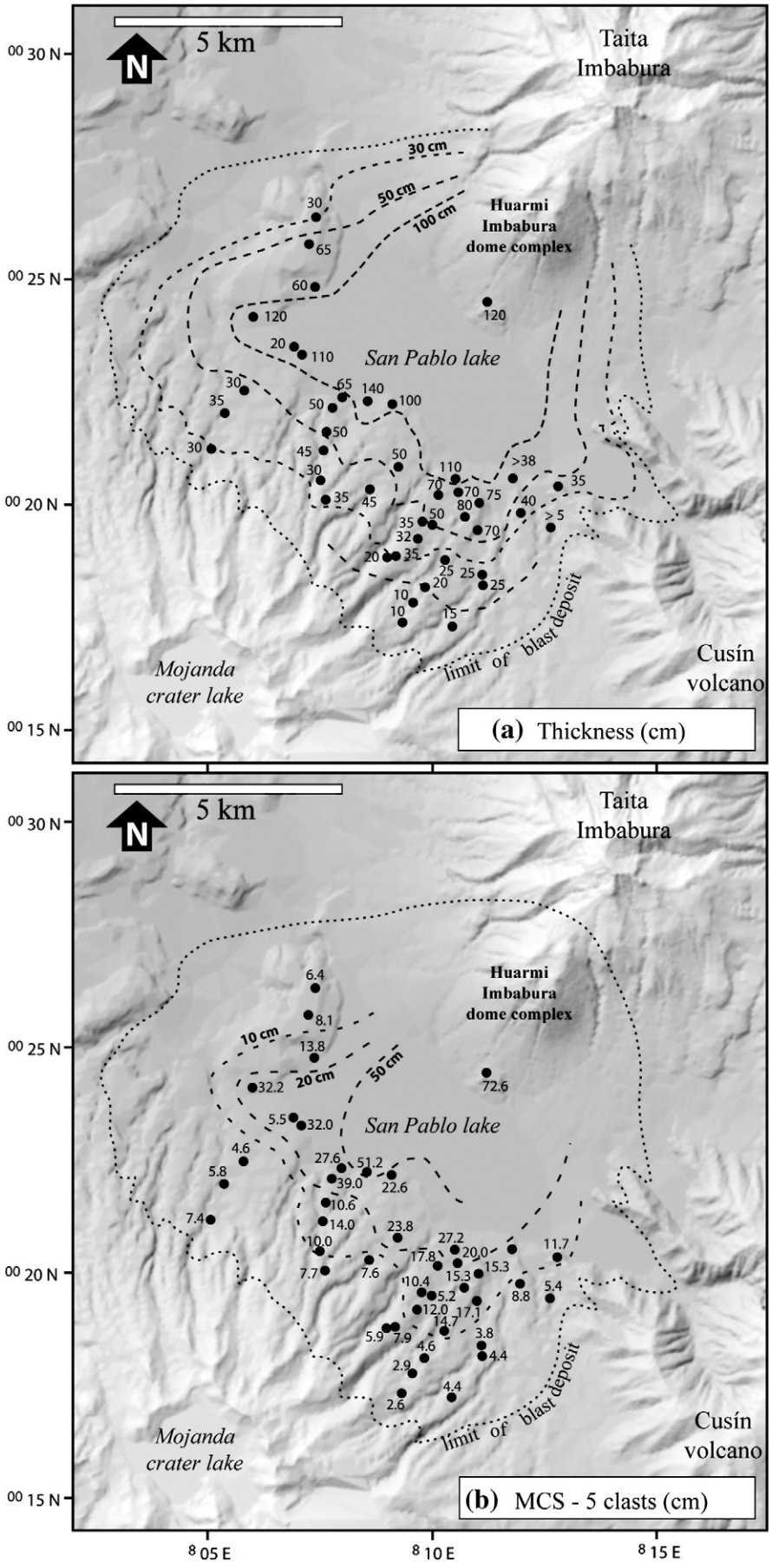
5 km
N
Taita
Imbabura
30 cm
50 cm
100 cm
Huarmi
Imbabura
dome complex
San Pablo lake
Mojanda
crater lake
limit of blast deposit
Cusín
volcano
(a) Thickness (cm)
10 cm
20 cm
50 cm
(b) MCS - 5 clasts (cm)
00 30 N
00 25 N
00 20 N
00 15 N
805 E
810 E
815 E

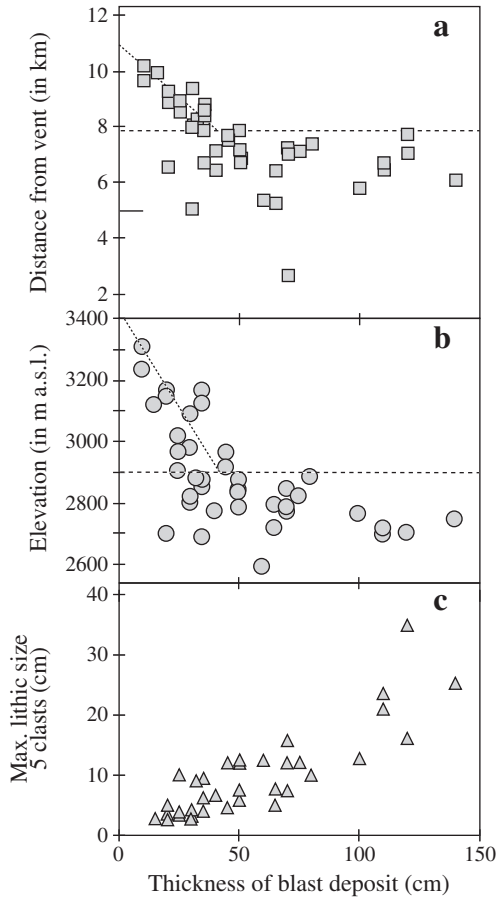

Fig. 9. Features of the blast deposit at Huarmi Imbabura. (a) and (b) are plots of distance and elevation versus thickness of the deposit, respectively. Thickness correlates to distance only beyond ~8 km, and elevation only above 2800 m asl. (c) Maximum lithic length (average of 5 largest clasts) versus measured thickness of the blast layer.

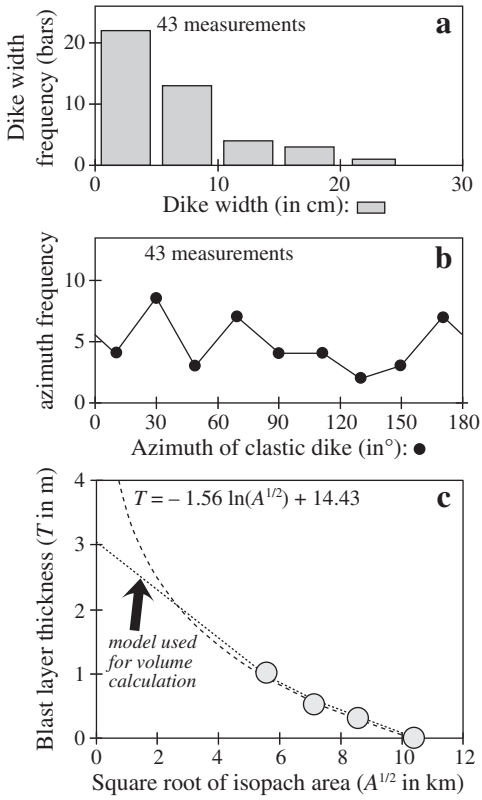

Fig. 10. Some features of the clastic dikes found below the blast deposit. (a) Plot of dike frequency against width. (b) Measured azimuth of 43 clastic dikes showing no preferential orientation and thus probable lack of tectonic control. (c) Plot of blast layer thickness against square root of isopach area. The data are well fitted by linear and logarithmic decay laws.

2010), Quilotoa (Hall and Mothes, 2008a), and Pululahua and Cuicocha (Hall et al., 2008). Imbabura's return rate as estimated here remains imprecise but points to major events separated by hundreds to thousands of years of dormancy, which contrasts with the high frequency pattern observed at the active volcanoes Cotopaxi (Hall and Mothes, 2008b) and Tungurahua (Hall et al., 1999; Le Pennec et al., 2008) in Ecuador's Eastern Cordillera, where the return rate is on the scale of decades to a few centuries. In summary, the geological history, the magmatic output rate, and the eruptive behavior argue for considering Imbabura as a potentially active volcano. At present Imbabura shows no fumarolic activity and the national seismic network maintained by IG-EPN shows no present seismic activity. However, the experience gained at other volcanoes such as Pinatubo, Chaitén and Sinabung indicates that the lack of seismic activity is not inconsistent with possible reactivation of apparently dormant edifices. A serious attention to monitoring may be required to anticipate future crises, especially where populations and infrastructure are important.

The present populations of the Imbabura region are unfamiliar with active volcanoes and essentially unprepared in case of unrest. Recently, a new volcano hazard map has been released (Ruiz et al., 2005) to popularize basic volcanological information to authorities and residents, and seismic monitoring has been initiated. Yet, an adequate strategy remains to be established by the authorities to control urban development in the volcano's periphery. The reactivation of the IVC after thousands of years of dormancy could include phreatic outbursts, directed explosions, pyroclastic flow and lava flow emplacements (Ruiz, 2003; Ruiz et al., 2003, 2005). The instability of the steeply inclined slopes at Taita, Huarmi dome and El Artezon cone and the formation of dangerous debris and mud flows after eruptive periods, all represent the principal hazards associated with this volcano.

7. Conclusion

We have presented the first radiometric evidence of late Pleistocene–early Holocene activity at Imbabura to conclude that it should be considered a potentially active volcano. Although the field and radiometric data support a low recurrence rate for its eruptions, most events of the past 35 ka cal BP involved significant magma volumes, resulting in an elevated output rate above 0.13 km^3/ka. Significant block-and-ash flow activity has repeatedly affected the eastern and northern flanks of Taita up until early Holocene times. A flank collapse and a major blast event were followed by extrusion of the large Huarmi dome complex in a relatively recent past, i.e. at ~30 ka cal BP. Similar eruptive behavior has been identified or inferred at other silicic volcanoes in Ecuador's Western Cordillera where no historic magmatic activity is documented (e.g. Quilotoa, Cuicocha, Pululahua, Atacazo, Chachimbiro).These findings substantiate the necessity of real-time monitoring of the IVC and serious civil defense planning.

The issues faced at Imbabura also apply to other volcanoes in the Ecuadorian arc where explosive Holocene activity has recently been confirmed by radiometric dating, especially along the Ecuadorian volcanic front, e.g. Chimborazo (Barba et al., 2008); Atacazo (Hidalgo et al., 2008); Chachimbiro (Bernard et al.—work in progress). Other volcanoes have a much more elevated level of activity than previously thought, e.g. Cayambe (Samaniego et al., 1998) and Cotopaxi (Hall and Mothes, 2008b). The Imbabura example thus raises the important

question of how to improve hazard preparedness of populations near volcanoes with low eruption return rates, and how to deliver adequate messages to help authorities' decisions in the development of urban areas and infrastructures near presently inactive but potentially dangerous volcanoes.

Acknowledgments

This work has been carried out in the context of a scientific cooperation program between the French IRD and the Instituto Geofisico, Escuela Politecnica Nacional Quito, Ecuador. Financial support for field work, ^{14}C dating and chemical analysis was provided by the IRD. All ^{14}C age determinations were performed by J. van der Plicht at the Center for Isotope Research, Gröningen University, The Netherlands. Chemical analysis by J. Cotten at the University of Bretagne Occidentale, Brest, France. Journal reviews by G. Zanchetta and an anonymous reviewer, and editorial handling by L Wilson were helpful to improve this paper. We dedicate this note to the memory of Dr. Jean-Philippe Eissen, who passed away during completion of this study.

References

Athens, J.S., 1999. Volcanism and Archaeology in the Northern Highlands of Ecuador. In: Mothes, P. (Ed.), Actividad volcánica y pueblos precolombinos en el Ecuador. Abya-Yala editions, Quito, pp. 157–189.
Bacon, C.R., Lanphere, M.A., 2006. Eruptive history and geochronology of Mount Mazama and the Crater Lake region, Oregon. Geol. Soc. Am. Bull. 118, 1331–1359.
Barba, D., Robin, C., Samaniego, P., Eissen, J.P., 2008. Holocene recurrent explosive activity at Chimborazo Volcano (Ecuador). J. Volcanol. Geotherm. Res. 176, 27–35.
Barberi, F., Coltelli, M., Ferrara, G., Innocenti, F., Navarro, J.M., Santacroce, R., 1988. Plio-Quaternary volcanism in Ecuador. Geol. Mag. 125, 1–14.
Boland, M.P., Pilatasig, L.F., Ibadango, C.E., M^{C}Court, W.J., Aspden, J.A., Hughes, R.A., Beate, B., 2000. Proyecto de Desarrollo Minero y Control Ambiental, Programa de Información Cartográfica y Geológico: Geology of the Western Cordillera between 0-1° N. Unpub. Report, CODIGEM – BGS, Quito.
Clapperton, C.M., 1990. Quaternary glaciations in the Southern Hemisphere: an overview. Quarter. Sci. Rev. 9, 229–304.
Clapperton, C.M., 1993a. Quaternary geology and geomorphology of South America. Elsevier, Amsterdam. 779 pp.
Clapperton, C.M., 1993b. Glacier readvances in the Andes at 12,500–10,000 yr BP: implications for mechanism of late—glacialclimatic change. J. Quarter. Sci. 8, 197–215.
Clapperton, C.M., Hall, M.L., Mothes, P., Hole, M.J., Still, J.W., Helmens, K.F., Kuhry, P., Gemmell, A.M.D., 1997. A younger Dryas icecap in the equatorial Andes. Quarter. Res. 47, 13–28.
Feeley, T.C., Davidson, J.P., 1994. Petrology of calc-alkaline lavas at Volcán Ollagüe and the origin of compositional diversity at Central Andean Stratovolcanoes. J. Petrol. 35, 1295–1340.
Féraud, G., Gastaud, J., Auzende, J.M., Olivet, J.L., Cornen, G., 1982. $^{40}Ar/^{39}Ar$ ages for the alkaline volcanism and the basement of the Gorringe Bank, North Atlantic Ocean. Earth Planet. Sci. Lett. 57, 211–226.
Fierstein, J., Nathenson, M., 1992. Another look at the calculation of fallout tephra volumes. Bull. Volcanol. 54, 156–167.
Froggatt, P.C., 1982. Review of methods estimating rhyolitic tephra volumes; applications to the Taupo Volcanic Zone, New Zealand. J. Volcanol. Geotherm. Res. 14, 1–56.
Hall, M.L., Beate, B., 1991. El volcanismo Plio-Cuaternario en los Andes del Ecuador; Paisaje Volcánico de la Sierra Ecuatoriana. In: Mothes, P. (Ed.), Estudios de Geografia, 4, pp. 5–17.
Hall, M.L., Mothes, P.A., 1996. El origen y la edad de la Cangahua superior, valle de Tumbaco (Ecuador). In: Zebrowski, C., Quantin, P., Trujillo, G. (Eds.), Proceedings of the III International Symposium on indurated volcanic soils, Quito, pp. 19–28.
Hall, M.L., Mothes, P.A., 2008a. Quilotoa volcano—Ecuador: an overview of the young dacitic volcanism in a lake-filled caldera. J. Volcanol. Geotherm. Res. 176, 44–55.
Hall, M., Mothes, P., 2008b. The rhyolitic-andesitic eruptive history of Cotopaxi Volcano, Ecuador. Bull. Volcanol. 70, 675–702. doi:10.1007/s00445-007-0161-2.
Hall, M.L., Robin, C., Beate, B., Mothes, P., Monzier, M., 1999. Tungurahua Volcano, Ecuador: structure, eruptive history and hazards. J. Volcanol. Geotherm. Res. 91, 1–21.
Hall, M.L., Samaniego, P., Le Pennec, J.L., Johnson, J., 2008. Ecuadorian Andes volcanism: a review of Late Pliocene to Present activity. J. Volcanol. Geotherm. Res. 176, 1–6. doi:10.1016/j.jvolgeores.2008.06.012.
Hidalgo, S., Monzier, M., Almeida, E., Chazot, G., Eissen, J.P., van der Plicht, J., Hall, M.L., 2008. Late Pleistocene and Holocene activity of Atacazo–Ninahuilca Volcanic Complex (Ecuador). J. Volcanol. Geotherm. Res. 176, 16–26.
Hildreth, W., Lanphere, M.A., 1994. Potassium-argon geochronology of a basalt-andesite-dacite arc system: the Mt. Adams volcanic field, Cascade Range of southern Washington. Geol. Soc. Am. Bull. 106, 1413–1429.
Hildreth, W., Fierstein, J., Lanphere, M., 2003. Eruptive history and geochronology of the Mount Baker volcanic field, Washington. Geol. Soc. Am. Bull. 115, 729–764.
Le Pennec, J.L., Jaya, D., Samaniego, P., Ramón, P., Moreno, S., Egred, J., van der Plicht, J., 2008. The AD 1300–1700 eruptive periods at Tungurahua volcano, Ecuador, revealed by historical narratives, stratigraphy and radiocarbon dating. J. Volcanol. Geotherm. Res. 176, 70–81.
Mahaney, W.C., Mliner, M.W., Kalm, V., Dirszowsky, W., Hancock, R.G.V., Beukens, R.P., 2008. Evidence for a Younger Dryas glacial advance in the Andes of northwestern Venezuela. Geomorpholgy 96, 199–211. doi:10.1016/j.geomorph.2007.08.002.
Newhall, C.G., Daag, A.S., Delfin, F.G. Jr., Hoblitt, R.P., McGeehin, J., Pallister, J.S., Regalado, T.M., Rubin, M., Tubianosa, B.S., Tamayo, R.A. Jr., Umbal, J.V., 1996. Eruptive history of Mount Pinatubo. In: Newhall C.G., Punongbayan R.S. (eds) Fire and Mud: Eruptions and Lahars of Mount Pinatubo, Philippines. Quezon City, Philippines: Philippine Institute of Volcanology and Seismology, and Seattle: University Washington Press, 165–195.
Reimer, P.J., Baillie, M.G.L., Bard, E., Bayliss, A., Beck, J.W., Blackwell, P.G., Bronk Ramsey, C., Buck, C.E., Burr, G.S., Edwards, R.L., Friedrich, M., Grootes, P.M., Guilderson, T.P., Hajdas, I., Heaton, T.J., Hogg, A.G., Hughen, K.A., Kaiser, K.F., Kromer, B., McCormac, F.G., Manning, S.W., Reimer, R.W., Richards, D.A., Southon, J.R., Talamo, S., Turney, C.S.M., van der Plicht, J., Weyhenmeyer, C.E., 2009. IntCal09 and Marine09 Radiocarbon Age Calibration Curves, 0–50,000 Years cal BP. Radiocarbon 51, 1111–1150.
Richards, J.P., Villeneuve, M., 2001. The Llullaillaco volcano, northwest Argentina: construction by Pleistocene volcanism and destruction by sector collapse. J. Volcanol. Geotherm. Res. 105, 77–105.
Robin, C., Hall, M.L., Jimenez, M., Monzier, M., Escobar, P., 1997. Mojanda volcanic complex (Ecuador): development of two adjacent contemporaneous volcanoes with contrasting eruptive styles and magmatic suites. J. S. Am. Earth Sci. 10, 345–359.
Robin, C., Samaniego, P., Le Pennec, J.L., Mothes, P., van der Plicht, J., 2008. Late Holocene cycles of dome growth and Plinian activity at Guagua Pichincha volcano (Ecuador). J. Volcanol. Geotherm. Res. 176, 7–15. doi:10.1016/j.jvolgeores.2007.10.008.
Robin, C., Eissen, J.P., Samaniego, P., Martin, H., Hall, M.L., Cotten, J., 2009. Evolution of the late Pleistocene Mojanda-Fuya Fuya volcanic complex (Ecuador), by progressive adakitic involvement in mantle magma sources. Bull. Volcanol. 71, 233–258. doi:10.1007/s00445-008-0219-9.
Robin, C., Samaniego, P., Le Pennec, J.L., Fornari, M., Mothes, P., van der Plicht, J., 2010. New radiometric and petrological constraints on the evolution of the Pichincha volcanic complex (Ecuador). Bull. Volcanol. 72, 1109–1129. doi:10.1007/s00445-010-0389-0.
Rodbell, D.T., Seltzer, G.O., 2000. Rapid ice margin fluctuations during the younger Dryas in the tropical Andes. Quarter. Res. 54, 328–338. doi:10.1006/qres.2000.2177.
Ruiz, A.G., 2003. Estudio Geovolcanológico del Complejo Volcánico Imbabura. Dissertation Msc., Escuela Politécnica Nacional, Quito, 318 pp.
Ruiz, A.G., Le Pennec, J.L., Hall, M.L., Eissen, J.P., Barba, D., 2003. Sintesis estratigrafica del complejo volcanico Imbabura. Quintas Jornadas en Ciencias de la Tierra, EPN Quito, pp. 19–22.
Ruiz, A.G., Le Pennec, J.L., Hall, M.L., Samaniego, P., 2005. Mapa de los peligros volcánicos potenciales del complejo volcánico Imbabura (scale; 1/50.000). Edit. IGM-IG/EPN-IRD.
Samaniego, P., Monzier, M., Robin, C., Hall, M.L., 1998. Late Holocene eruptive activity at Nevado Cayambe Volcano, Ecuador. Bull. Volcanol. 59, 451–459.
Samaniego, P., Martin, H., Monzier, M., Robin, C., Fornari, M., Eissen, J.-P., Cotten, J., 2005. Temporal evolution of magmatism at Northern Volcanic Zone of the Andes: the geology and petrology of Cayambe volcanic complex (Ecuador). J. Petrol. 45, 2225–2252.
Siebert, L., Simkin, T., Kimberly, P., 2011. Volcanoes of the World, Third Edition. University of California Press. 568 pp.
Simkin, T., Siebert, L., 1994. Volcanoes of the World. Smithsonian Institution, Washington, DC. 349 pp.
Steiger, R.H., Jäger, E., 1977. Subcommission on Geochronology: convention on the use of decay constants in geo- and cosmochronology. Earth Planet. Sci. Lett. 36, 359–362.
Stothers, R.B., 1984. The Great Tambora Eruption of 1815 and Its Aftermath. Science 224, 1191–1198.
Stuiver, M., Reimer, P.J., 1993. Extended 14C database and revised CALIB radiocarbon calibration program. Radiocarbon 35, 215–230.
Stuiver, M., Reimer, P.J., Reimer, R.W., 2005. CALIB 6.0. [WWW program and documentation].
Szakács, A., 1994. Redefining active volcanoes: a discussion. Bull. Volcanol. 56, 321–325.
Thouret, J.-C., 1999. Volcanic geomorphology—an overview. Earth Sci. Rev. 47, 95–131.
Thouret, J.-C., Van der Hammen, T., Salomons, B., Juvigné, E., 1996. Paleoenvironmental changes and glacial stades of the last 50,000 years in the Cordillera Central, Colombia. Quarter. Res. 46, 1–18.
Thouret, J.-C., Dávila, J., Rivera, M., Gourgaud, A., Eissen, J.P., Le Pennec, J.L., Juvigné, E., 1997. The largest explosive eruption (VEI 6) in historical times (1600 AD) in the Central Andes at Huaynaputina, Southern Peru. C. R. Acad. Sci. Paris 325, 931–938.
Tonneijck, F.H., van der Plicht, J., Jansen, B., Verstraten, J.M., Hooghiemstra, H., 2006. Radiocarbon dating of soil organic matter fractions in andosols in northern Ecuador. Radiocarbon 48, 337–353.
von Hillebrandt, C., 1989. Estudio geovolcanológico del complejo volcánico Cuicocha-Cotacachi y sus aplicaciones, Provincia de Imbabura. Dissertation Msc., Escuela Politécnica Nacional, Quito.
von Hillebrandt, C., Beate, B., Hall, M., 1991. Mapa de los peligros volcánicos potenciales asociados con el Volcán Imbabura, Provincia de Imbabura (1:50.000). Instituto Geofísico, Escuela Politécnica Nacional, Quito.
Watt, S.F.L., Pyle, D.M., Mather, T.A., Martin, R.S., Matthews, N.E., 2009. Fallout and distribution of volcanic ash over Argentina following the May 2008 explosive eruption of Chaitén, Chile. J. Geophys. Res. 114, B04207. doi:10.1029/2008JB006219.